CFD ANALYSIS OF CROSSWIND EFFECTS ON A PASSENGER CAR TRAVELING NEAR A CONTAINER TRUCK

PHÂN TÍCH BẰNG MÔ PHỎNG CFD ẢNH HƯỞNG CỦA GIÓ NGANG ĐẾN XE CON KHI LƯU THÔNG GẦN XE CONTAINER

Pham Van Tinh, Pham Hai Dang, Nguyen Duy Quang, Tran Cong Chi, Nguyen Van Tuu*

Vietnam National University of Forestry, Vietnam

*Corresponding author: nguyenvantuu.vnuf@gmail.com

(Received: March 22, 2026; Revised: May 10, 2026; Accepted: May 22, 2026)

DOI: 10.31130/ud-jst.2026.24(5A).169E

Abstract - This study uses Computational Fluid Dynamics (CFD) to investigate the aerodynamic characteristics of a passenger car under crosswind conditions, both in isolation and when traveling alongside a container truck. Simulations were performed by keeping the resultant freestream velocity magnitude constant at 120 km/h, while changing the inlet-flow direction to impose yaw angles of 0°, 15°, 30°, 45°, and 60°. The drag coefficient (C_D), lift coefficient (C_L), side force coefficient (C_S), and yaw moment coefficient (C_n) were evaluated. The results show that, C_D increased monotonically with yaw angle in both cases. C_L reached its maximum at 45°, while C_S reached its largest magnitude around 30°-45°. C_n increased up to 45° before decreasing at 60°. In the case of traveling alongside a container truck, the aerodynamic coefficients were generally lower due to the shielding effect of the container truck.

Key words - Crosswind; aerodynamics; passenger car; vehicle interaction; CFD simulation

Tóm tắt - Nghiên cứu này sử dụng Động lực học lưu chất tính toán (CFD) để khảo sát các đặc tính khí động học của xe con dưới điều kiện gió ngang, trong hai trường hợp đơn lẻ và khi di chuyển song song với xe container. Các mô phỏng được thực hiện trong điều kiện cố định độ lớn vận tốc ở 120 km/h, đồng thời thay đổi hướng dòng vào để tạo các góc lệch hướng gió 0°, 15°, 30°, 45° và 60°. Hệ số cản khí động (C_D), hệ số lực nâng (C_L), hệ số lực ngang (C_S) và hệ số mô men quay đầu (C_n) được đánh giá. Kết quả cho thấy, C_D tăng đơn điệu theo góc lệch hướng gió trong cả hai trường hợp. C_L đạt giá trị lớn nhất tại 45°, trong khi C_S đạt độ lớn lớn nhất trong khoảng 30°–45°. C_n tăng đến 45° trước khi giảm tại 60°. Trong trường hợp di chuyển song song với xe container, hệ số khí động học nhìn chung thấp hơn do hiệu ứng che chắn của xe container.

Từ khóa - Gió ngang; khí động lực học; xe con; tương tác khí động giữa các xe; mô phỏng CFD

1. Introduction

When a vehicle travels on the road, the interaction between the airflow and the vehicle body generates aerodynamic forces and moments that directly affect driving stability, safety, and energy consumption. At high speeds, aerodynamic drag becomes a dominant component of the total resistance, while lift and side forces significantly influence vehicle handling and stability, particularly under crosswind conditions.

Over the past decades, vehicle aerodynamics has been extensively studied using both experimental and numerical approaches [1, 2]. Traditionally, wind tunnel experiments have been the primary method for evaluating aerodynamic performance and deriving empirical correlations for different vehicle geometries. However, with the rapid advancement of computational resources, Computational Fluid Dynamics (CFD) has become a standard tool for predicting aerodynamic characteristics with high flexibility and reduced cost. In particular, Reynolds-Averaged Navier–Stokes (RANS) models are widely used in automotive aerodynamics due to their balance between computational efficiency and acceptable accuracy for turbulent flows [3-5].

Recent research has focused on improving aerodynamic performance through geometric optimization and flow control strategies. A significant number of studies have demonstrated that reducing flow separation and vortex structures in the rear region of the vehicle is critical for minimizing pressure drag [6, 7]. Additionally, the influence of the front-end design, including the windshield inclination, hood curvature, and air intake regions, has been widely investigated [8, 9]. More recently, attention has also been directed toward underbody flow, wheel aerodynamics, and surface details, as these factors can substantially alter the overall flow structure around the vehicle [10, 11].

In addition to single-vehicle aerodynamics, increasing attention has been given to the aerodynamic interaction between multiple vehicles. Several studies have investigated the effects of vehicle proximity, overtaking maneuvers, and platooning configurations on aerodynamic forces [12, 13]. These studies indicate that the wake generated by a leading vehicle can significantly influence the flow field of a following vehicle, leading to variations in drag reduction or amplification depending on the relative position and spacing. Moreover, when two vehicles travel side by side, strong flow acceleration and pressure gradients may occur in the gap region, resulting in increased lateral forces and potential stability issues [14].

Crosswind effects represent another critical aspect of vehicle aerodynamics. Under crosswind conditions, the flow becomes highly asymmetric, leading to increased side force and yawing moment. Previous studies have shown that crosswind can induce significant changes in aerodynamic coefficients, especially for bluff bodies and high-profile vehicles such as trucks and buses [15, 16]. The

magnitude of these effects strongly depends on the yaw angle, vehicle geometry, and flow conditions.

Despite the substantial body of research on vehicle aerodynamics, studies that simultaneously consider both crosswind effects and aerodynamic interaction between different types of vehicles - such as passenger cars and heavy-duty container trucks - remain relatively limited. In real highway conditions, passenger cars frequently operate in close proximity to large vehicles, where the combined effects of wake interaction, pressure asymmetry, and crosswind can significantly alter the aerodynamic loads acting on the car. These complex interactions may lead to increased lateral instability and safety risks, especially at high speeds.

In Vietnam, several studies have applied CFD techniques to analyze the aerodynamic characteristics of various vehicle types, including buses, electric vehicles, and container trucks [17-20]. While these studies provide valuable insights into flow structures and aerodynamic coefficients, they primarily focus on isolated vehicles and do not fully address multi-vehicle interaction under crosswind conditions.

Therefore, this study aims to investigate the aerodynamic characteristics of a passenger car traveling in proximity to a container truck under crosswind conditions using CFD simulations in SolidWorks. The analysis focuses on key aerodynamic coefficients, including drag (C_D), lift (C_L), side force (C_S), and the yaw moment coefficient (C_n) of the passenger car. These parameters are evaluated to quantify the combined effects of vehicle interaction and crosswind on aerodynamic performance, lateral stability, and yawing behavior.

2. Methodology

2.1. Vehicle Geometry and Simplified Models

The passenger car is represented by its actual geometry. The 3D CAD model is created based on the manufacturer's specifications and is simplified by removing minor details such as door handles, side mirrors, and antennae (Figure 1). These features have a negligible impact on the overall aerodynamic forces but can significantly increase computational costs. The model has overall dimensions of approximately 4.17 meters in length, 1.67 meters in width, and 1.50 meters in height.

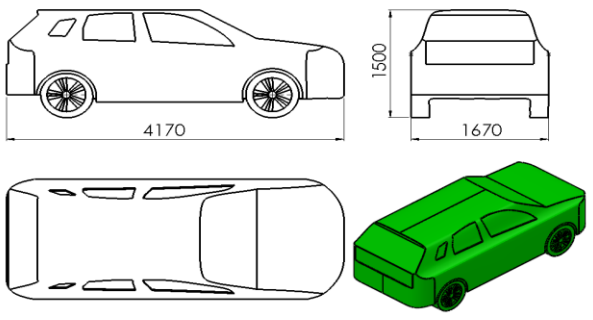

Figure 1. *Simplified geometrical model of the passenger car*

The container truck is represented by a simplified geometric model based on a heavy vehicle design. This model features a rectangular bluff body with rounded front corners and a box-shaped rear container truck, as illustrated in Figure 2. This simplified representation effectively captures the key aerodynamic characteristics of heavy vehicles, including the presence of large wake regions, significant exposure of side surfaces to crosswinds, and the effects of underbody flow. The dimensions of the container truck are a total length of 15.90 meters, a width of 2.55 meters, and a height of 4.10 meters.

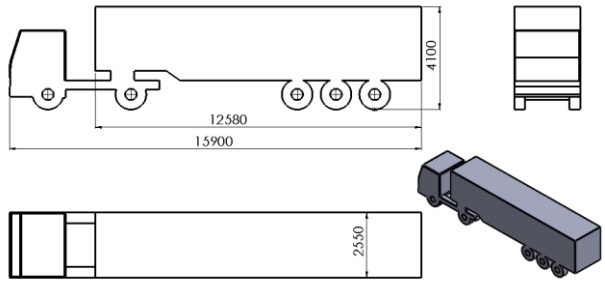

Figure 2. *Simplified geometrical model of the container truck*

2.2. Computational Domain and Boundary Conditions

The computational domain is constructed as a three-dimensional rectangular enclosure surrounding both the passenger car and the container truck, as shown in Figure 3. The domain dimensions are defined explicitly based on the global coordinate system used in the simulation. In the present setup, the domain extends 12 m upstream, 24 m downstream, 5 m in the lateral direction, and 22 m in the vertical direction, ensuring sufficient space for flow development while minimizing blockage effects and artificial acceleration of the flow.

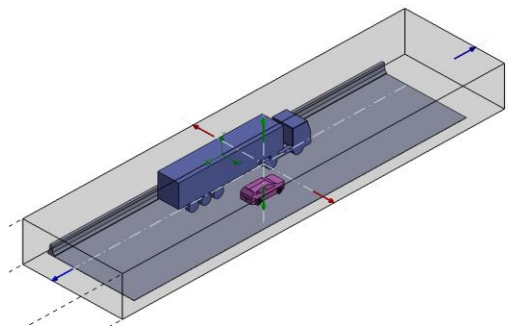

Figure 3. *Computational domain and boundary condition setup*

Within the computational domain, the relative positioning of the vehicles is defined to represent a realistic highway driving condition. The lateral spacing between the passenger car and the container truck is fixed at 1.5 m. In addition, the container truck is positioned at a distance of 1.0 m from the road barrier, representing the influence of roadside constraints on the flow field. This configuration ensures consistent geometric conditions for evaluating aerodynamic interaction between the two vehicles.

A velocity-inlet boundary condition was applied at the upstream boundary of the computational domain. In this study, the velocity of 120 km/h refers to the resultant freestream velocity magnitude rather than the longitudinal vehicle speed. The yaw angle (ψ) is defined as the angle between the inlet velocity vector and the longitudinal axis of

the passenger car. For each prescribed ψ, the inlet velocity vector was decomposed into lateral and longitudinal components, while the magnitude V = 120 km/h was kept constant for all simulation cases. This boundary treatment supports a stable and consistent comparative simulation of airflow interaction between the passenger car and the container truck under crosswind conditions.

The outlet boundary is specified as a pressure outlet with ambient static pressure of 101325 Pa, allowing the flow to exit the computational domain without artificial reflection. All vehicle surfaces, including both the passenger car and the container truck, as well as the road barrier, are treated as no-slip walls, ensuring zero velocity at the surface and enabling accurate prediction of boundary layer development and flow separation. The road surface is modeled as a stationary wall with a no-slip condition. Although a moving ground condition can provide higher fidelity, the stationary ground assumption is adopted in this study to reduce computational complexity while maintaining acceptable accuracy for comparative aerodynamic analysis.

The upper and lateral boundaries of the computational domain are defined as far-field or symmetry-equivalent conditions to minimize boundary-induced disturbances and approximate an open external-flow environment. This configuration ensures a stable and physically representative simulation of airflow interaction between the passenger car and the container truck under crosswind conditions.

2.3. Mesh Generation

The computational mesh is generated using the automatic meshing scheme in SolidWorks Flow Simulation, with a global mesh level set to 6. Local mesh refinement is applied to selected faces of the vehicle surfaces and interaction regions between the passenger car and the container truck. The local refinement level is set to 7, with additional channel refinement enabled to improve resolution in narrow gaps and underbody flow regions.

Advanced refinement is activated with a minimum gap size of approximately 3.76×10^{-4}m and a refinement angle of about 0.318 rad, allowing better capture of sharp gradients and flow separation near geometric features. These settings ensure enhanced accuracy in predicting vortex structures and wake development. The influence of mesh density on the predicted aerodynamic quantities was further evaluated through a mesh independence study.

2.4. Turbulence Model and Solver Settings

The working fluid is defined as air and modeled as an incompressible ideal gas under standard atmospheric conditions, with a reference pressure of 101325 Pa and temperature of 293.2 K.

The numerical simulations were performed using a steady-state Reynolds-Averaged Navier–Stokes (RANS) approach implemented in SolidWorks Flow Simulation. Turbulence effects were modeled using the built-in modified k-ε turbulence model, which is suitable for external aerodynamic applications involving separated turbulent flows.

The governing equations were discretized using the finite volume method on a Cartesian-based computational mesh with local mesh refinement in regions of strong flow interaction and wake development. Automatic adaptive refinement was employed to improve the resolution of velocity gradients and vortex structures. The inlet turbulence intensity and turbulence length scale were specified as 0.1% and 0.016 m, respectively, representing low ambient turbulence conditions typical of highway environments.

2.5. Simulation Cases

To evaluate the aerodynamic behavior of a passenger car under crosswind conditions, a structured set of numerical simulations is conducted. The study focuses on two main scenarios: (i) an isolated passenger car and (ii) a passenger car interacting with a container truck in a side-by-side configuration.

In the first scenario, the passenger car is modeled as a single vehicle subjected to crosswind angles (ψ) of 0°, 15°, 30°, 45°, and 60°. These cases provide baseline aerodynamic characteristics for comparison. In the second scenario, the passenger car travels parallel to a container truck, representing a typical side-by-side driving condition on highways. The same set of crosswind angles (0°, 15°, 30°, 45°, and 60°) is applied to ensure consistency and enable direct comparison with the baseline case.

All simulations were conducted using an inlet velocity of 120 km/h. The yaw angles of 0°, 15°, 30°, 45°, and 60° were imposed by changing the direction of the inlet velocity vector, enabling direct comparison between the isolated-car and car–container truck interaction cases under comparable dynamic-pressure conditions.

2.6. Convergence Criteria and Evaluation Parameters

To ensure the reliability and accuracy of the numerical simulations, appropriate convergence criteria are established for all cases. The solution is considered converged when the residuals of the governing equations are sufficiently reduced, and the monitored aerodynamic quantities exhibit stable behavior over successive iterations.

In addition to residual monitoring, the convergence of key aerodynamic coefficients is carefully evaluated. Specifically, the C_D, C_L, C_S and C_n of the passenger car are tracked throughout the simulation process. Convergence is assumed when the variations of these coefficients fall below 0.5% over several consecutive iterations.

Since the incoming flow is inclined with respect to the vehicle's longitudinal axis under crosswind conditions, the drag and side forces are not directly taken as the force components along the global coordinate axes. Instead, the resultant aerodynamic force is projected onto the freestream direction and the lateral direction normal to the freestream. Therefore, the aerodynamic coefficients are defined as follows:

$$C_D = \frac{-F_X \sin\,\psi + F_Z \cos\,\psi}{\frac{1}{2}\rho V^2 A} \tag{1}$$

$$C_L = \frac{F_Y}{\frac{1}{2}\rho V^2 A} \tag{2}$$

$$C_S = \frac{F_X \cos\psi - F_Z \sin\psi}{\frac{1}{2}\rho V^2 A} \quad (3)$$

$$C_n = \frac{M_Y}{\frac{1}{2}\rho V^2 A L} \quad (4)$$

where F_X, F_Y, and F_Z are the aerodynamic force components along the lateral, vertical, and longitudinal directions, respectively (N); M_Y is the yaw moment about the vertical axis (N.m); ψ is the yaw angle (deg) (Figure 4); ρ is the air density (kg/m³); V is the inlet velocity magnitude (m/s); A is the reference frontal area of the passenger car (m²); and L is the characteristic vehicle length (m). The frontal area A is determined from the projected frontal area of the passenger car model, while L is taken as the overall vehicle length. All aerodynamic coefficients are dimensionless.

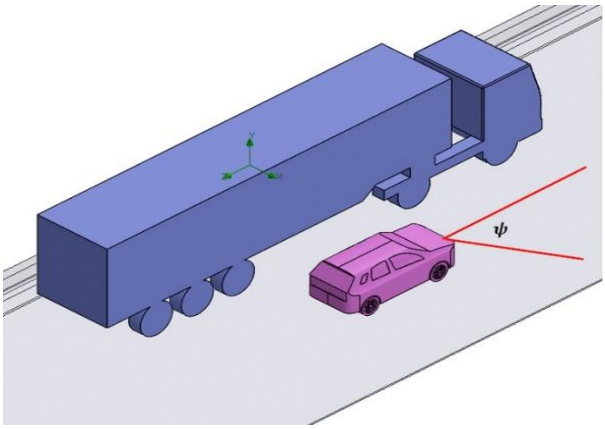

Figure 4. *Coordinate system and yaw angle (ψ) for the passenger car under crosswind conditions*

3. Results and Discussion

3.1. Numerical Validation and Convergence Analysis

3.1.1. Validation of the Numerical Model

To evaluate the reliability of the numerical methodology, the predicted aerodynamic characteristics of the isolated passenger car were compared with previously published CFD studies on passenger vehicles. In particular, the validation focused on the C_D, which is one of the most commonly used parameters for aerodynamic assessment and numerical verification in automotive applications [1, 21, 22]. Table 1 summarizes the comparison between the present study and selected published results reported in the literature.

Table 1. *Comparison of C_D with previously published studies*

Study	Vehicle model / condition	C_D
Wang, et al. [1]	Typical passenger vehicle models	0.28–0.38
Yuan, et al. [21]	Passenger vehicle under crosswind	0.40–0.46
Zhou, et al. [22]	Ahmed body with wheelhouse configurations	0.423–0.442
Present study	Isolated passenger car	0.437

The results indicate that the predicted C_D is consistent with previously reported values for passenger vehicle aerodynamics under crosswind conditions. Minor discrepancies are mainly due to differences in vehicle geometry, mesh resolution, turbulence modeling, and flow conditions, confirming the reliability of the adopted numerical approach.

3.1.2. Mesh Independence and Convergence Behavior

To ensure the reliability of the numerical simulations, both mesh independence and convergence behavior were carefully examined for the passenger car–container truck interaction case under crosswind conditions. A mesh independence study was conducted using three different mesh densities, namely coarse, medium, and fine meshes. The comparison was performed at a yaw angle of 60°, representing the most critical aerodynamic condition considered in this study. The C_D of the passenger car was selected as the primary evaluation parameter due to its relatively stable behavior and widespread use in vehicle aerodynamic validation.

The results in Table 2 indicate that the predicted drag coefficient gradually converges with increasing mesh density. The relative difference between the medium and fine meshes was approximately 4.54%, indicating that the numerical solution became reasonably stable with mesh refinement. Therefore, the medium mesh configuration was selected for all subsequent simulations to achieve a reasonable balance between computational accuracy and computational cost.

Table 2. *Mesh independence study for the passenger car–container truck interaction case at $\psi = 60°$*

Mesh level	Global mesh level	Total cells	C_D	Relative difference (%)
Coarse	5	62363	0.893	2.06
Medium	6	157116	0.875	4.54
Fine	7	420177	0.837	–

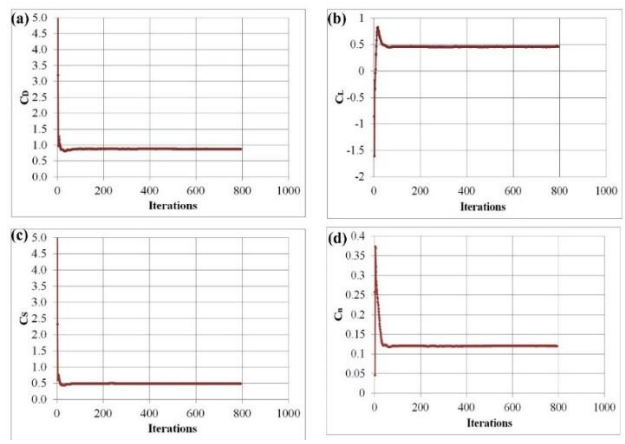

Figure 5. *Convergence histories of the aerodynamic coefficients of the passenger car in the passenger car–container truck interaction case: (a): C_D; (b): C_L; (c): C_S; and (d): C_n at $\psi = 60°$*

In addition to mesh independence, the convergence behavior of the numerical solution was also examined. Figure 5 presents the convergence histories of the aerodynamic coefficients acting on the passenger car in the passenger car–container truck interaction case at a yaw angle of 60°. At the initial stage of the simulation (first 50–100 iterations), all monitored coefficients exhibit

significant fluctuations due to the rapid adjustment of the flow field from the initial conditions. In particular, C_D shows a sharp decrease from a high initial value before stabilizing, while C_L and C_S experience noticeable transient oscillations. C_n also varies significantly during this stage, reflecting the sensitivity of moment-related quantities to the evolving pressure distribution.

After approximately 100 iterations, all coefficients gradually converge toward steady values. From 200 iterations onward, only minor fluctuations around the mean values are observed, indicating that the flow field has reached a stable state. Among the monitored quantities, the drag coefficient stabilizes more rapidly, whereas the yaw moment coefficient requires slightly more iterations to converge due to its higher sensitivity to small variations in the flow structure.

Overall, the convergence behavior demonstrates that the numerical setup is stable and capable of producing reliable aerodynamic predictions. The same convergence criteria are consistently applied to all simulation cases, ensuring the comparability of the results presented in this study.

3.2. Effect of Crosswind Angle on Aerodynamic Coefficients

The aerodynamic coefficients of the passenger car under different crosswind angles for both the isolated and passenger car–container truck interaction cases are summarized in Table 3.

Table 3. *Comparison of aerodynamic coefficients under different crosswind angles*

Coefficient	Case	0°	15°	30°	45°	60°
	Isolated	0.437	0.638	0.936	1.229	1.419
C_D	Interaction	0.353	0.443	0.604	0.743	0.875
	ΔC_D (%)	-19.3	-30.5	-35.4	-39.5	-38.3
	Isolated	0.099	0.359	0.716	0.869	0.541
C_L	Interaction	0.067	0.175	0.378	0.573	0.463
	ΔC_L (%)	-32.8	-51.2	-47.2	-34.1	-14.3
	Isolated	0.016	-0.751	-1.231	-1.229	-0.859
CS	Interaction	0.030	-0.439	-0.763	-0.743	-0.488
	ΔC_S (%)	89.7	-41.6	-38.0	-39.5	-43.1
	Isolated	-0.0031	0.107	0.196	0.215	0.162
Cn	Interaction	-0.0033	0.065	0.128	0.153	0.120
	ΔCn (%)	6.5	-39.1	-34.6	-28.9	-26.0

For both simulation cases, C_D generally increases with increasing yaw angle due to the enlarged projected frontal area and intensified flow separation under crosswind conditions. This trend can be attributed to the stronger impingement of the incoming flow on the side surface of the passenger car, which increases the effective area exposed to the flow and may enlarge the separated wake region. Consequently, the pressure-drag contribution becomes more pronounced, which is consistent with the increasing trend of C_D under larger yaw angles.

In the isolated-car case, C_D rises from 0.437 at 0° to 1.419 at 60°. A similar trend is observed in the interaction case, where C_D increases from 0.353 to 0.875 over the same yaw-angle range. However, the presence of the container truck significantly reduces C_D at all investigated yaw angles. Compared with the isolated-car case, C_D decreases by approximately 19.3%–39.5%, with the largest reduction occurring at 45°. This behavior indicates that the truck generates a pronounced shielding effect that partially protects the passenger car from direct crosswind exposure.

The lift coefficient also exhibits a nonlinear variation with yaw angle. This behavior can be attributed to the yaw-induced redistribution of surface pressure around the car body, which modifies the vertical pressure imbalance and hence the net lift force. In the isolated-car case, C_L increases from 0.099 at 0° to a peak value of 0.869 at 45°, before decreasing to 0.541 at 60°. A similar trend is observed in the interaction case, where C_L reaches a maximum value of 0.573 at 45°. Compared with the isolated-car case, the interaction configuration decreases C_L by approximately 14.3%–51.2%, depending on the yaw angle. This reduction may be associated with the modified wake and pressure field generated by the container truck, which can reduce the vertical pressure imbalance around the passenger car and consequently lower the vertical aerodynamic loading.

The side-force coefficient shows strong sensitivity to crosswind conditions. Because C_S takes negative values for most yaw-angle cases in the present coordinate system, the physical severity of lateral aerodynamic loading should be interpreted using its magnitude. In the isolated-car case, C_S rapidly changes from 0.016 at 0° to -1.231 at 30°, indicating substantial lateral aerodynamic loading under moderate crosswind conditions. This large side-force magnitude is mainly associated with the pressure imbalance between the windward and leeward sides of the passenger car under yawed incoming flow. In the interaction case, the magnitude of C_S is consistently smaller for ψ from 15° to 60°. The largest reduction is observed at 60°, where C_S decreases by approximately 43.1% compared with the isolated-car case. This behavior indicates that the container truck modifies the surrounding flow field and generates a shielding effect that reduces direct crosswind impact on the passenger car. As a result, the lateral pressure difference across the passenger car is weakened, leading to a lower side-force magnitude in the interaction case. At $\psi = 0°$, C_S remains close to zero in both cases, and the observed variation mainly results from numerical asymmetry and wake interaction effects.

The yaw moment coefficient is closely related to the side-force behavior but is also affected by the location of the resultant aerodynamic force relative to the vehicle reference point. In the isolated-car case, C_n increases from nearly zero at 0° to a maximum value of 0.215 at 45°, before decreasing slightly to 0.162 at 60°. This trend may be associated with the combined effects of lateral-force magnitude, pressure-center displacement, and the corresponding aerodynamic moment arm. At ψ = 45°, the combined effect of strong lateral loading and an increased pressure-center offset produces the largest yawing moment. In the interaction case, C_n remains consistently lower at all investigated crosswind angles above 0°. Compared with the isolated-car case, C_n decreases by approximately 26.0%–39.1%, indicating that the

aerodynamic interaction with the container truck alleviates the yawing tendency induced by crosswind. This reduction can be attributed to the weakened pressure asymmetry around the passenger car caused by the wake and shielding effects generated by the upstream truck.

3.3. Flow Field Analysis and Aerodynamic Interaction

The variations in the aerodynamic coefficients are closely related to the evolution of the flow field structure, as illustrated by the velocity streamlines and pressure distributions in Figures 6 and 7. The results show that the container truck significantly modifies the surrounding flow field and influences the aerodynamic behavior of the passenger car under crosswind conditions.

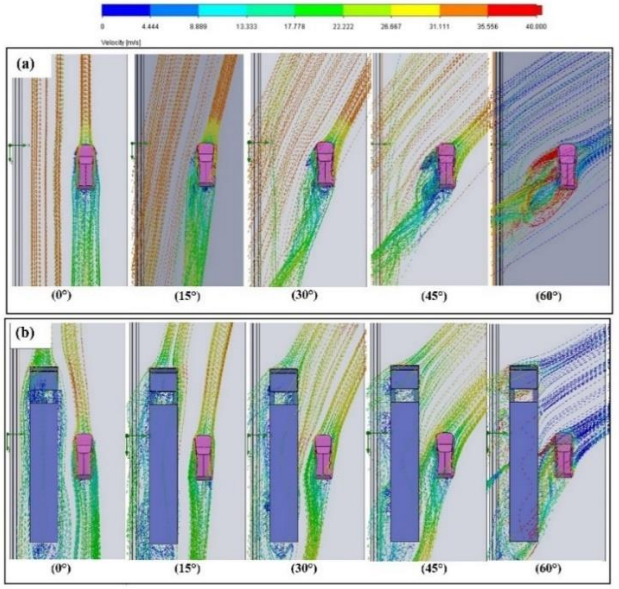

Figure 6. *Flow field and velocity distribution around a passenger car under different crosswind angles: (a) isolated passenger car case (b): passenger car–container truck interaction case*

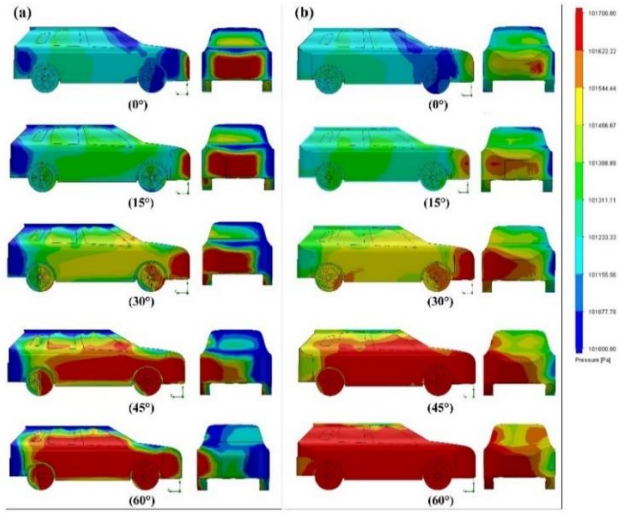

Figure 7. *Surface pressure on the passenger car under different crosswind angles: (a): isolated passenger car case (b): passenger car–container truck interaction case*

At 0°, the flow field remains nearly symmetric in both cases. The streamlines indicate relatively attached flow with a small wake region behind the vehicle, while the pressure contours show a typical distribution with a high-pressure region at the frontal surface and relatively uniform pressure along the side surfaces. In the interaction case, the truck produces only a minor influence on the passenger car because the crosswind effect is weak.

As the yaw angle increases from 15° to 30°, the flow field becomes increasingly asymmetric. In the isolated-car case, larger wake regions and stronger flow separation develop on the leeward side, accompanied by intensified pressure differences between the windward and leeward surfaces. The velocity streamlines exhibit significant lateral deflection, indicating the increasing influence of crosswind. In contrast, the interaction case shows weaker wake structures and reduced pressure asymmetry around the passenger car because part of the incoming airflow is blocked by the container truck.

At high yaw angles of 45°and 60°, strong flow separation and large-scale vortex structures dominate the flow field. In the isolated-car case, extensive low-pressure regions form on the side and rear surfaces, resulting in significant increases in aerodynamic loading. However, in the interaction case, the container truck generates a pronounced wake region that partially shields the passenger car from direct crosswind exposure. As shown in Figures 6(b) and 7(b), the reduced velocity magnitude and weaker pressure asymmetry around the passenger car are consistent with the reductions observed in C_D, C_L, C_S, and C_n. The shielding effect becomes particularly evident at 60°, where the truck wake strongly modifies the surrounding flow structure and reduces the aerodynamic loads acting on the passenger car.

In the interaction case, increasing yaw angle leads to stronger flow separation, larger wake regions, and more complex vortex structures around the passenger car–truck system. These flow characteristics intensify aerodynamic disturbances and may adversely affect vehicle stability and controllability under strong crosswind conditions. However, compared with the isolated-car case, the container truck generates a shielding effect that partially reduces direct crosswind exposure and weakens the aerodynamic loads acting on the passenger car, particularly at high yaw angles.

4. Conclusion

This study investigated the aerodynamic characteristics of a passenger car under crosswind conditions using CFD simulations for both isolated-car and passenger car–container truck interaction cases. The results showed that increasing the yaw angle noticeably influenced the aerodynamic behavior of the passenger car. C_D increased monotonically with yaw angle in both cases. C_L reached its maximum at 45°, while C_S reached its largest magnitude around 30°– 45°. C_n increased up to 45° before decreasing at 60°.

Compared with the isolated-car case, the passenger car–container truck interaction case generally produced lower aerodynamic coefficients due to the shielding effect of the container truck. This suggests that the container truck partially reduced the direct crosswind exposure of the passenger car under the investigated side-by-side

configuration. Flow-field analysis also revealed modified wake structures, pressure asymmetry, and vortex interaction between the two vehicles under crosswind conditions.

There are several limitations to this study. The simulations were performed at a fixed resultant freestream velocity rather than at a fixed longitudinal vehicle speed with an additional lateral wind component. Therefore, the results should be interpreted as a comparative yawed-flow analysis rather than a direct reproduction of all real-road crosswind conditions. The simulations did not consider transient wind fluctuations, rotating wheels, moving-ground effects, suspension motion, or vehicle steering response, all of which may influence the unsteady aerodynamic loads under real driving conditions. In addition, simplified traffic scenarios and fixed relative vehicle positions were adopted, which may not fully represent realistic highway interactions. Future work should therefore incorporate transient simulations, moving vehicle dynamics, moving-ground and rotating-wheel conditions, and experimental validation to improve prediction accuracy under real operating conditions.

Acknowledgment: This research was conducted at the Vietnam National University of Forestry. The author would like to express sincere gratitude to the editorial board and the reviewers for their valuable comments and constructive suggestions, which significantly improved the quality of the manuscript.

REFERENCES

[1] Y. Wang, Y. Xin, Z. Gu, S. Wang, Y. Deng, and X. Yang, "Numerical and experimental investigations on the aerodynamic characteristic of three typical passenger vehicles," *Journal of Applied Fluid Mechanics,* vol. 7, no. 4, pp. 659-671, 2014.

[2] J. Piechna, "A review of active aerodynamic systems for road vehicles," *Energies,* vol. 14, no. 23, p. 7887, 2021.

[3] A. Misar, P. Davis, and M. Uddin, "On the effectiveness of scale-averaged rans and scale-resolved iddes turbulence simulation approaches in predicting the pressure field over a nascar racecar," *Fluids,* vol. 8, no. 5, p. 157, 2023.

[4] S. N. A. Yusuf, Y. Asako, N. A. C. Sidik, S. B. Mohamed, and W. M. A. A. Japar, "A short review on rans turbulence models," *CFD letters,* vol. 12, no. 11, pp. 83-96, 2020.

[5] P. Ekman, D. Wieser, T. Virdung, and M. Karlsson, "Assessment of hybrid RANS-LES methods for accurate automotive aerodynamic simulations," *Journal of Wind Engineering and Industrial Aerodynamics,* vol. 206, p. 104301, 2020.

[6] R. D. R. Mariaprakasam, S. Mat, P. M. Samin, N. Othman, M. Ab Wahid, and M. Said, "Review on flow controls for vehicles aerodynamic drag reduction," *Journal of Advanced Research in Fluid Mechanics and Thermal Sciences,* vol. 101, no. 1, pp. 11-36, 2023.

[7] M. G. Connolly, A. Ivankovic, and M. J. O'Rourke, "Drag reduction technology and devices for road vehicles-A comprehensive review," *Heliyon,* vol. 10, no. 13, pp. 1-19, 2024.

[8] C. Gao, "Effect of front windshield angle on drag coefficient of electric vehicles," *Theoretical and Natural Science,* vol. 12, no. 1, pp. 101-107, 2023.

[9] M. Elrawemi and İ. I. Aburawey, "The effect of front and rear windscreen angles on the aerodynamic drag force of a simplified car model," *International Journal of Energy Applications and Technologies,* vol. 6, no. 3, pp. 83-88, 2019.

[10] E. Josefsson, S. Sebben, and M. Urquhart, "Characterisation of the flow around passenger vehicle wheels with varying tyre profiles," *International Journal of Heat and Fluid Flow,* vol. 103, p. 109191, 2023.

[11] Z. Yuan and Y. Wang, "Effect of underbody structure on aerodynamic drag and optimization," *Journal of Measurements in Engineering,* vol. 5, no. 3, pp. 194-204, 2017.

[12] M. Syafiq, I. A. Ishak, M. Arafat, R. Abd Rashid, N. E. Othman, Z. M. Salleh, and S. F. Z. Abidin, "Computational Fluid Dynamics Analysis of Aerodynamic Characteristics on Overtaking Vehicles in Crosswind Conditions," *International Journal of Automotive and Mechanical Engineering,* vol. 22, no. 2, pp. 12373-12387, 2025.

[13] Q. Zhao, B. Wang, Y. Lu, X. Liao, Y. Xianyu, and T. Huang, "Aerodynamic Stability Analysis of Vehicles under Vehicle Meeting Conditions Based on Aerodynamics and Multi-body Dynamics Coupling," *Journal of Applied Fluid Mechanics,* vol. 19, no. 3, pp. 308-321, 2026.

[14] J. Bunker and A. Parajuli, "Examining lateral positions of cars and heavy vehicles on a two lane, two way motorway," *Transport Engineering in Australia,* vol. 10, no. 2, pp. 129-139, 2006.

[15] A. Yudianto, H. Sofyan, and N. A. Fauzi, "Aerodynamic characteristics of overtaking bus under crosswind: CFD investigation," *CFD Letters,* vol. 14, no. 8, pp. 20-32, 2022.

[16] D. Alic, A. Miltenovic, M. Banic, and R. V. Zafra, "Numerical investigation of large vehicle aerodynamics under the influence of crosswind," *Spectrum of Mechanical Engineering and Operational Research,* vol. 2, no. 1, pp. 13-23, 2025.

[17] A. N. Nguyen, H. Q. Le, P. H. Tran, Q. T. Hoang, and D. H. Chu, "Study on the Body Aerodynamics Improvements of the Electric Vehicle HaUI-EV2," *Hanoi University of Industry Journal of Science and Technology,* vol. 55, pp. 91-94, 2019.

[18] T. L. Phan, "Evaluating the Influence of Different Types of Unstructured Mesh In the Simulation Automotive Aerodynamic Simulation," *The University of Danang - Journal of Science and Technology,* vol. 22, no. 5A, pp. 17-22, 2024.

[19] L. B. Pham and V. S. Pham, "A Numerical Modeling Study For Automotive Aerodynamic Noise," *Journal of Marine Science and Technology,* vol. DB, pp. 368-376, 2021.

[20] T. L. Nguyen, C. C. Tran, V. T. Nguyen, and K. N. Nguyen, "Determining optimal parameters affecting dynamic drag forces on an electric car body," *Journal of Forestry Science and Technology* vol. 14, no. 1, pp. 146-153, 2025.

[21] Z. Yuan, Z. Gu, Y. Wang, and X. Huang, "Numerical investigation for the influence of the car underbody on aerodynamic force and flow structure evolution in crosswind," *Advances in Mechanical Engineering,* vol. 10, no. 10, pp. 1-14, 2018.

[22] H. Zhou, Q. Chen, R. Qin, L. Zhang, and H. Li, "Investigation of wheelhouse shapes on the aerodynamic characteristics of a generic car model," *Advances in Mechanical Engineering,* vol. 13, no. 12, pp. 1-13, 2021.